6. The future of strong lensing

CHRIS FASSNACHT

We are on the verge of an explosion in data volume owing to recently started or upcoming surveys of the skies. One of the benefits of these new programmes will be the vastly increased number of known strong gravitational lens systems. In this chapter I will discuss three main topics: lens discovery in these surveys; the use of lensing to determine the mass distribution in galaxies, and in particular substructure in massive galaxy haloes; and cosmological measurements with large lens samples.

6.1. Introductory remarks

The next few decades will present an especially exciting time for strong gravitational lensing. This is because a combination of new instrumentation and, in some cases, brand new telescopes have come online, or are at an advanced stage of planning. With the enhanced observing capability enabled by these new facilities, a number of large-scale astronomical surveys are planned. These surveys will provide unprecedented combinations of depth, area, angular resolution and, in some cases, will open up poorly explored wavelength regimes. As a result, they should lead to orders of magnitude increases in the number of known strong lens systems. Indeed, although dedicated observational surveys for lenses have proved productive in the past, it is likely that the vast majority of future lenses will be discovered by mining the data produced by the new large surveys. The resulting large samples of lenses will lead to two major advantages: (1) improved statistics for investigations of galaxy properties, evolution in these properties and cosmology etc., and (2) the discovery of rare lens systems that are especially interesting and useful. As a complement to the large surveys, the planned construction of significantly larger ground- and space-based telescopes will provide enhanced follow-up capabilities of the new discoveries. Furthermore, advances in modelling and analysis codes will allow researchers to exploit more of the information available in observations of lens systems.

As is obvious at this point, this chapter has a focus on the field of strong gravitational lensing, and how it can be affected by large recently started and upcoming astronomical surveys. Taking this approach necessarily ignores other aspects of lensing that also have an exciting future. The new surveys will have a strong impact on investigations that utilize weak lensing or microlensing. For discussions of science that can be done in these fields, the reader is referred to the chapters by Schneider and Wambsganss in this book, as well as comprehensive discussions in the *Euclid* 'Red Book' (Laureijs et al. 2011), and the Large Synoptic Survey Telescope (LSST) Science Book (Abell et al. 2009).

6.2. Techniques for finding strong lens systems

The early observational history of strong lensing comprised serendipitous discoveries, as well as a few small-scale observing programmes that were dedicated to finding lenses (e.g. Hewitt et al. 1989; Bahcall et al. 1992; Wisotzki et al. 2002; Myers et al. 2003; Browne et al. 2003). The number of known strong lens systems increased from one in 1979 (Walsh, Carswell and Weymann 1979) to ∼20 by the mid 1990s to ∼100 by the early

Astrophysical Applications of Gravitational Lensing, ed. E. Mediavilla et al. Published by Cambridge University Press.

2000s. An enormous step forward came with the release of the Sloan Digital Sky Survey data (SDSS; York et al. 2000). This new data set led to roughly a doubling of the number of known lenses, the majority of which were found through the spectroscopic survey that became the Sloan Lens Advanced Camera for Surveys (SLACS) Survey (e.g. Bolton et al. 2004, 2006). The lesson that can be drawn from this is that the appearance of a new large and high-quality data set can produce a significant number of new lens discoveries, even if the motivation for conducting the survey had no direct focus on lensing.

In this section I will discuss how to find strong lenses in large surveys. Most of the methods discussed involve at some stage a process of visual inspection. In this step, each object in the target sample is examined by a person who essentially performs a rough lens modelling process in their head. Objects for which it appears that a plausible lens model can explain the system morphology, colours, etc., are then flagged and passed to the next step, which is typically some kind of additional observational follow-up as well as a more quantitative modelling of the system.

6.2.1 *The most basic approach*

At its most basic level, a lens survey can be described as the following steps:

Survey observations → Visual inspection → Follow-up

In this brute force approach, every object in a survey is visually inspected. An example of this was the search for lenses in the COSMOS (Scoville et al. 2007) survey by Jackson (2008), who looked at more than 285 000 objects and found 70 lenses, three of which were new compared to the earlier, more focused, search of COSMOS by Faure et al. (2008). Although Jackson was able to examine 8000–10 000 objects per hour, this approach soon becomes untenable for large surveys.

6.2.2 *Down-selecting to a target population*

Most lens searches reduce the number of objects that need to be viewed by a person, by focusing either on the objects that are most likely to be acting as lenses or on those that are most likely to be lensed. Thus, the process becomes either:

Target selection → Survey observations → Visual inspection → Follow-up

or

Survey observations → Target selection → Visual inspection → Follow-up

with the first of these processes being most commonly used for the early surveys for lenses (e.g. Hewitt et al. 1989; Bahcall et al. 1992; Wisotzki et al. 2002; Myers et al. 2003; Browne et al. 2003) and the second now more commonly used with the existence of large survey databases such as SDSS (York et al. 2000), CFHTLS,[†] etc. In these approaches, it is most efficient to choose the rarer of the two potential target populations. For example, for the lens searches in the GOODS (Fassnacht et al. 2004) and COSMOS (Faure et al. 2008) fields, the objects most likely to be the lensing objects (luminous red galaxies) are

[†] Canada–France–Hawaii Telescope Legacy Survey; http://www.cfht.hawaii.edu/Science/CFHLS/.

far outnumbered by probable background sources (faint blue galaxies). Thus, both of these searches focused on potential lensing galaxies, and in the case of COSMOS reduced the number of objects that needed to be examined from >285 000 to ∼9000 (Faure et al. 2008), while still finding the vast majority of the lenses discovered by the broader search of Jackson (2008). Another example of a search focused on the lensing objects is the Sloan Giant Arcs Survey (SGAS; e.g. Hennawi et al. 2008; Bayliss et al. 2011), in which ∼40 000 galaxy clusters that have been selected from SDSS data by the red sequence technique are viewed by four independent examiners and graded based on their likelihood of containing a giant arc. The process is enhanced by an interactive tool that presents colour images of each system and re-introduces a subset of systems with rotations and translations to test the robustness of the scoring system. Follow-up with the Nordic Optical Telescope of the highest-rated systems shows that the selection produces good purity, with >90% of candidates being confirmed as lens systems.

Other lens searches focus on the lensed sources, when these are likely to be rare. As an example of this type of survey, consider the Cosmic Lens All-Sky Survey (CLASS; Myers et al. 2003; Browne et al. 2003). This project selected a sample of flat-spectrum radio sources from low-resolution data. This sample of targets was then observed at higher angular resolution by the VLA. By working at radio wavelengths, CLASS had the advantages of consistently high angular resolution (∼0.25 arcsec), no confusion by emission from the lensing galaxy, and simple source morphology since snapshot images of flat-spectrum radio sources typically show a single unresolved component (Figure 6.1). Thus, it was very simple to quickly examine the 10 000 objects in the survey and select the small number showing multiple components for follow-up. The final yield of CLASS and its earlier and smaller counterpart JVAS (Jodrell Bank-VLA Astrometric Survey; Patnaik et al. 1992; Browne et al. 1998; Wilkinson et al. 1998) was 22 lens systems (Browne et al. 2003), which is still the largest sample of lensed radio-loud AGN. Other surveys have followed a similar approach by targeting bright quasars at optical wavelengths (e.g. Bahcall et al. 1992; Maoz et al. 1993; Wisotzki et al. 2002).

6.2.3 *Further refinement of the target population*

With the increasingly large number of objects in survey databases, even choosing to focus on either the lenses or on the lensed sources may still result in an overwhelming number of systems to visually inspect. Therefore, recent lens surveys have introduced a further level of refinement in order to produce a more manageable number of targets. Thus, the process becomes:

$$\text{Survey observations} \rightarrow \text{Target selection} \rightarrow \text{Target refinement} \rightarrow \text{Visual inspection} \rightarrow \text{Follow-up}$$

This further refinement is necessarily done via some kind of quantitative cut. Below we will explore some of the approaches taken. This is far from an exhaustive list, but will serve to illustrate some of the refinement techniques.

6.2.3.1 Extended objects with quasar colours

In this approach the initial target population is quasars, selected from a large imaging survey by virtue of their colours. The search for lenses can then be conducted in two complementary ways, using catalogues of source properties generated from the survey data. The first looks for nearby, but separate, objects that have the same colours as the target quasar. These systems are wide-separation lens candidates. The second evaluates

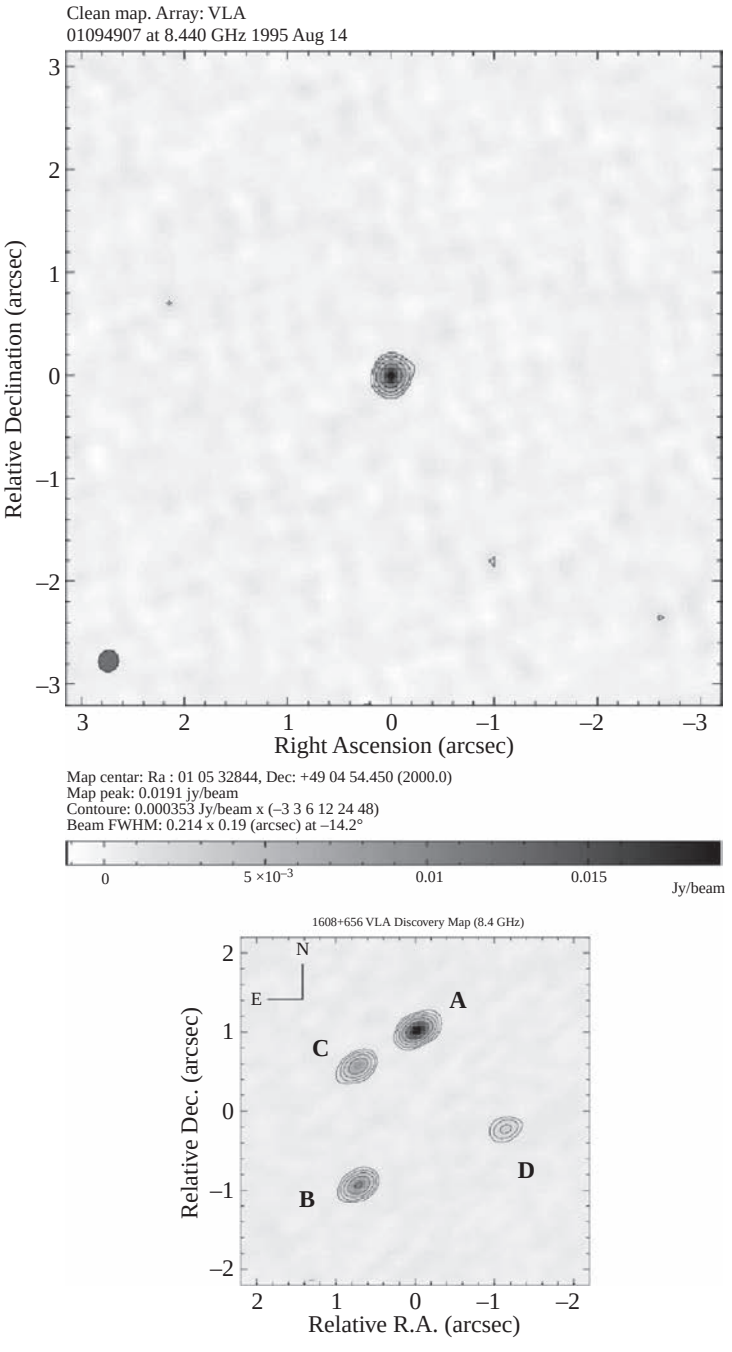

FIGURE 6.1. Example of the data from CLASS. Top: a typical flat spectrum radio source, in which the emission seen in a short exposure is dominated by a single point-like component. Bottom: a gravitational lens found in CLASS, where the short exposure reveals multiple point-like components.

the morphology of the target objects. If they are extended, i.e. poorly fitted by the point-spread function (PSF) of the observations, they are candidate lens systems for which the image separation is small compared to the seeing. This is exactly the approach taken by the SDSS Quasar Lens Survey (SQLS; Oguri et al. 2006, 2008; Inada et al. 2008, 2010, 2012). Starting with a quasar catalogue of over 100 000 objects (Schneider et al. 2010) generated from the SDSS data set (York et al. 2000), their approach created a refined target sample of 520 candidates, of which 26 are lens systems (Inada et al. 2012). This method is easily extendable to the next generation of surveys.

6.2.3.2 Blue rings around red galaxies

Another refinement of the target population can be achieved by performing an automated selection of blue arcs or rings around red galaxies. One such approach has been conducted in the RingFinder implementation in the Strong Lensing Legacy Survey (SL2S; Cabanac et al. 2007; Ruff et al. 2011; Gavazzi et al. 2012), which is conducted in the Wide Survey area of the CFHTLS. Here the initial target population is early-type galaxies, selected as galaxies that are both bright and red. The refinement consists of taking the difference between the bluer (g-band) and redder (r-band) images of these galaxies, tuned such that the galaxies subtract away well in the redder image. The new target population is then automatically selected by using the properties of the residual image in the bluer band. The selection is based on the number of significantly positive pixels in, and the morphology of, the residuals, where the evaluation criteria focus on arc- or ring-like residuals. It is at this point that the visual inspection enters. This automated refinement is effective in reducing the number of target objects. From 3700 early-type galaxies per square degree, the ring search reduces the number of targets to 18 per square degree (Gavazzi et al. 2012). This reduction makes the visual inspection tenable, at least for the CFHTLS-Wide Survey, which has an area of ∼171 square degrees. After inspection, 2–3 high-quality candidates per square degree are then passed to the follow-up stage. Approximately 50% of the high-quality candidates so far have been confirmed as lens systems (Ruff et al. 2011; Gavazzi et al. 2012). For larger future surveys, however, even this significant reduction in targets may still lead to unmanageably large numbers for the visual inspection step.

6.2.3.3 Spectroscopic selection

One of the most powerful lens-search techniques utilizes spectroscopy. The premier example of this is the project that became the Sloan Lens ACS Survey (SLACS; Bolton et al. 2004, 2006). The idea behind this approach is to automatically examine spectra of the initial target sample, which for SLACS were primarily luminous red galaxies (LRGs) from the SDSS. Spectra that exhibited emission lines that were at a different, higher, redshift than that of the initially targeted LRG were flagged as lens candidates. Since the SDSS fibres were 3 arcseconds in diameter, this emission must be coming from a nearby object, which could be lensed by the LRG. The initial spectroscopic search found 49 candidates from ∼51 000 targets (Bolton et al. 2004) and further candidates were revealed by later analyses. The final yield of SLACS was 85 definite lenses and 13 additional likely lens systems (Auger et al. 2009), which effectively doubled the existing sample of known lenses. The SLACS approach is now being extended to higher redshifts through the BOSS Emission Line Lens Survey (BELLS; Brownstein et al. 2012), where the initial data set comes from the Baryon Oscillation Spectroscopic Survey data set (BOSS; Eisenstein et al. 2011). This programme has found 44 lenses in its initial search and expects the final survey to yield several hundred new lens systems when completed (Brownstein et al.

2012). Even though this process has led to the most significant increase in the numbers of currently known lenses, it will not produce any large (i.e. order of magnitude) further increases until a next-generation wide-area spectroscopic survey has been conducted.

6.2.3.4 Extended variable objects

The methods discussed above have used morphologies, colours and spectra to search for new lens systems. However, some of the current and upcoming surveys will add an exciting new dimension that can also be exploited for finding lenses, namely the time domain. One method for doing so was described by Pindor (2005), who suggested that repeated imaging of a field might lead to the discovery of lensed quasars through their time delays. The idea would be to find nearby point sources, i.e. those with separations typical of a galaxy-scale lens, and to look for delays that would cause their light curves to be well matched. Systems satisfying these criteria would have a high probability of being lenses. The other technique that has been proposed to find lens systems via time-domain information is that of Kochanek et al. (2006a), which uses difference imaging to search for lensed quasars. Whereas supernovae and AGN will show up in difference imaging as point sources, lensed quasars will appear as extended objects in the difference imaging. This characteristic makes such a search very efficient and should lead to high-purity samples of lens candidates for areas at high galactic latitudes. An application of this technique was performed in the SDSS Supernova Survey region, and correctly recovered a previously known lens system (Lacki et al. 2009).

6.2.4 *Moving into the future: massive numbers of target objects*

While the methods discussed in the previous section have been used successfully to search for lenses, the number of targets for visual inspection that will be produced by future surveys will make such searches overly time consuming for small groups of researchers. Strong lensing is an inherently rare event, with ∼10–20 lenses per square degree found in the moderately deep and high-resolution *HST* imaging examined for the COSMOS (Faure et al. 2008) and HAGGLeS (Marshall et al. 2009) lens searches. Although the current and very near-term surveys will not achieve this combination of depth and angular resolution, later surveys will. For example, both *Euclid* and the Square Kilometre Array (SKA) should achieve angular resolutions of ∼0.2 arcseconds and cover significant fractions of the sky. Similarly, the LSST, while not reaching the angular resolutions of *Euclid* and SKA, will cover half the sky with sub-arcsecond seeing. The selection of an initial target population of early-type galaxies from these surveys will produce samples of $\sim 10^7$ initial targets. Even with the target refinement techniques discussed in the previous section, the surveys will produce on the order of 10^{5-6} targets for visual inspection.

6.2.5 *Lens searches in future surveys*

As is clear, the trend in the upcoming sky surveys is to produce an embarrassment of riches in terms of lens searches. If the surveys open up a new region of parameter space, such as a new wavelength regime or the time domain, it may be possible to use the existing techniques to quickly 'skim the cream' by selecting a sample of high-probability lens candidates (e.g. the SPT sample described in Section 6.3). However, in most cases the number of potential candidates, even with the target refinement techniques mentioned above, will far exceed the ability of typical groups of investigators to evaluate in the usual techniques. What is needed is either (1) some kind of automation of the by-eye modelling that occurs in most of the existing methods, or (2) a vast increase in the number of eyes

that are examining the targets. Work in both of these areas is proceeding and will set the stage for the upcoming data onslaught.

6.2.5.1 Automated lens modelling

In almost all of the lens-search techniques described above, there is a step at which a person looks at the target and does a rough mental lens modelling in order to classify the target as a potential lens or not. Thus, one of the approaches to dealing with future survey data is to have this modelling step be performed automatically by a 'robot' that evaluates the targets. Things that are likely to be lenses are those objects for which a lens model can reproduce the observed emission to some degree of precision. The advantages of this approach are that it will be consistent across the sample, unaffected by boredom or tiredness, will be repeatable and can be tuned to various levels of optimism (set by what fraction of the targets are expected to be lenses). The highest-ranked candidates from the robot classification can then be evaluated by the investigators, who will have a much smaller data set with which to deal. The automated lens modelling approach has been tested by the HAGGLeS team (Marshall et al. 2009), who applied it to data residing in the *HST* archive. All exposures obtained with ACS above a minimum exposure time in at least two bands were evaluated by the robot. Several new lens candidates have been discovered by this technique (Marshall et al., in preparation).

6.2.5.2 Citizen science

The other technique for dealing with the huge new data sets is to vastly increase the number of people that are looking at the targets. This can be achieved by harnessing the large numbers of people worldwide who are not professional astronomers but who have a keen interest in astronomy. With the proper web-based interface, this 'citizen science' approach can produce impressive results. Perhaps the best-known of these projects is the 'Galaxy Zoo', where members of the public determined the morphological classification of galaxies in the SDSS (e.g. Lintott et al. 2008). A similar project has been developed to search for lens candidates under the Zooniverse programme that grew out of Galaxy Zoo. The 'Space Warps' project[†] has recently been started and lens classification is under way.

6.3. The dawn of a new era

Having described methods for discovering new lens systems, let us turn to the data sets in which these searches will be taking place. What makes the current epoch so exciting is that a number of new surveys have either recently started or will do so within the next decade or two. These surveys will open up new paths for lens discoveries through significant increases in area, depth and angular resolution. Additionally, new wavelength regimes are being opened up for lens searches and follow-up observations. An especially exciting aspect of some of the new surveys is their time-domain information.

The properties that enhance the ability of a survey to successfully find a large number of new lenses include:

Depth. The objects being lensed are often faint and at high redshift. Even with the magnification produced by the lensing process, these can fall below the flux limit of a survey. Thus, there can a strong benefit to pushing the detection limit of a survey to

[†] http://spacewarps.org.

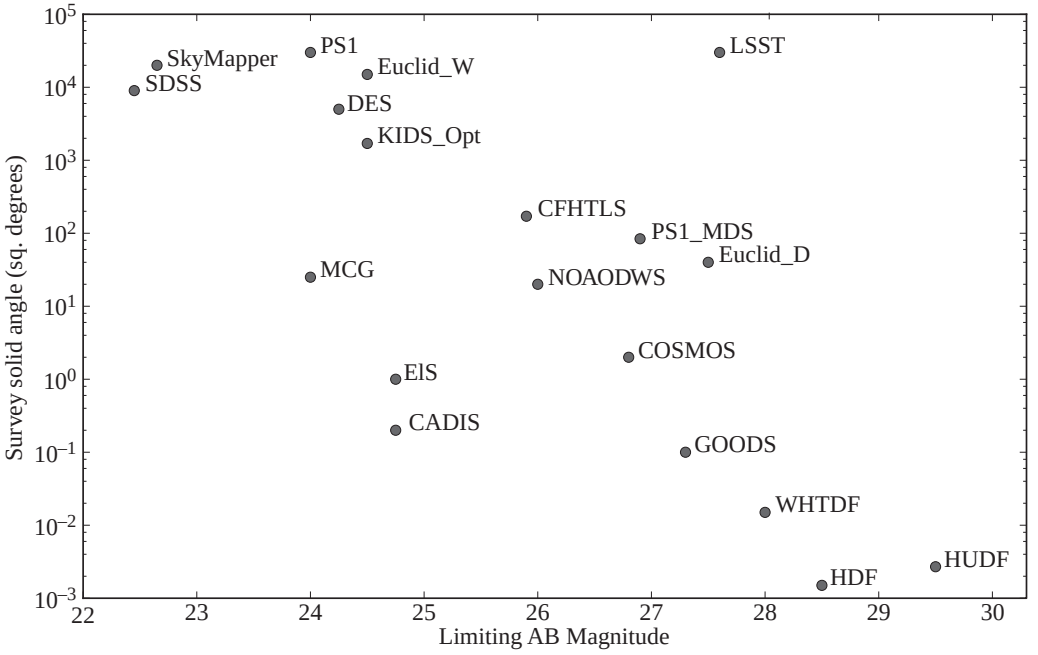

FIGURE 6.2. Plot of survey area vs. depth for a selection of existing or planned surveys. Note that *locations of the points should be taken as rough estimates*, especially the limiting magnitudes, since some approximations were necessary to bring all of the magnitudes onto the same system. Data taken from the summary in the LSST Science Book (Abell et al. 2009) and survey web pages. Survey abbreviations are: SDSS: Sloan Digital Sky Survey, MCG: Millennium Galaxy Catalogue, PS1: Pan-STARRS-1 wide survey, DES: Dark Energy Survey, KIDS_Opt: KIDS Optical Survey, Euclid_W: Euclid Wide Survey, EIS: ESO Imaging Survey, CADIS: Calar Alto Deep Imaging Survey, CFHTLS: Canada–France–Hawaii Telescope Legacy Survey, NOAODWS: NOAO Deep Wide Survey, PS1_MDS: Pan-STARRS-1 Medium-deep Survey, GOODS: Great Observatories Origins Deep Survey, Euclid_D: Euclid Deep Survey, WHTDF: William Herschel Telescope Deep Field, HDF: Hubble Deep Field, HUDF: Hubble Ultra-Deep Field.

fainter values, depending on the slope of the number counts in the flux range of interest. Of course, there is a trade-off between depth and area that needs to be considered in the survey design. Figure 6.2 shows the decisions that were made by various survey programmes based on time available, cost and science goals.

High angular resolution. Typical galaxy-scale strong lenses produce image separations of ∼1 arcsecond. Thus, any search for strong lenses will need sub-arcsecond resolution across the survey area. For ground-based surveys obtained in variable seeing, it may be necessary to follow up lens candidates with higher-resolution observations, either in the best seeing, or by using adaptive optics observations, or by going to space-based observations. A further advantage of high-resolution observations is that, for faint objects in background-limited observations, the higher resolution pulls more of the flux into the central portions of the objects and makes them easier to detect (Figure 6.3).

Wide area. Strong gravitational lens systems are rare objects. At the depth and resolution provided by a typical 1–2 orbit *HST* observation, there are expected to be ∼10 lenses per square degree. Thus, for a significant increase over the ∼200 known strong lenses,

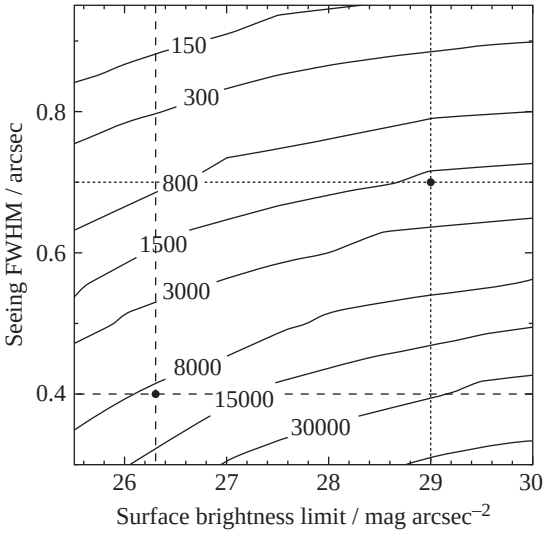

FIGURE 6.3. Example of the effects of angular resolution on a lens survey. Contours show number of galaxy–galaxy strong lenses expected in the LSST survey. The dashed lines show the approximate expected surface brightness limit for one visit and typical seeing expected for the best visit on a field. The dotted lines mark the median seeing for the survey and the approximate surface brightness limit of the 10-year stacked image. The improved seeing in the single visit can more than compensate for the brighter detection limit. (Figure from LSST Science Book, used by permission from Phil Marshall.)

surveys will have to cover at least several hundred square degrees. For surveys with depth or angular resolution that is worse than the canonical *HST* values, larger survey areas will be needed.

Time-domain information. Although this has not been much of a consideration in past lens surveys, some of the new surveys will have time-domain information. This allows variability-based lens searches to be conducted (e.g. Section 6.2.3.4). Currently, the Panoramic Survey Telescope and Rapid Response System (Pan-STARRS) is conducting the first major sky survey that explicitly exploits the time domain. In particular, the '3π' survey will cover the entire sky at declinations $\delta > -30$, with each field being observed 60 times, 12 times in each of five filters: u, g, r, i and z. On a longer time scale, the LSST will also cover over 20 000 square degrees in six filters, going deeper than Pan-STARRS. The combination of deep data, good angular resolution for a ground-based telescope and excellent time sampling over the 10-year project lifetime will provide a rich data set for lensing investigations.

Exploring a new wavelength regime. Improvements in instrumentation and the construction of new telescopes has meant that surveys at wavelengths that were relatively unexplored in the past can now be conducted. The advantage of opening up a new region of parameter space in this way is that it may be possible to quickly select the most probable lens candidates by straightforward target refinement. An example is the survey at mm wavelengths conducted by the South Pole Telescope (Carlstrom et al. 2011). An examination of the number counts reveals an excess of high-flux sources that, when followed up at high angular resolution with ALMA (Atacama Large Millimeter Array),

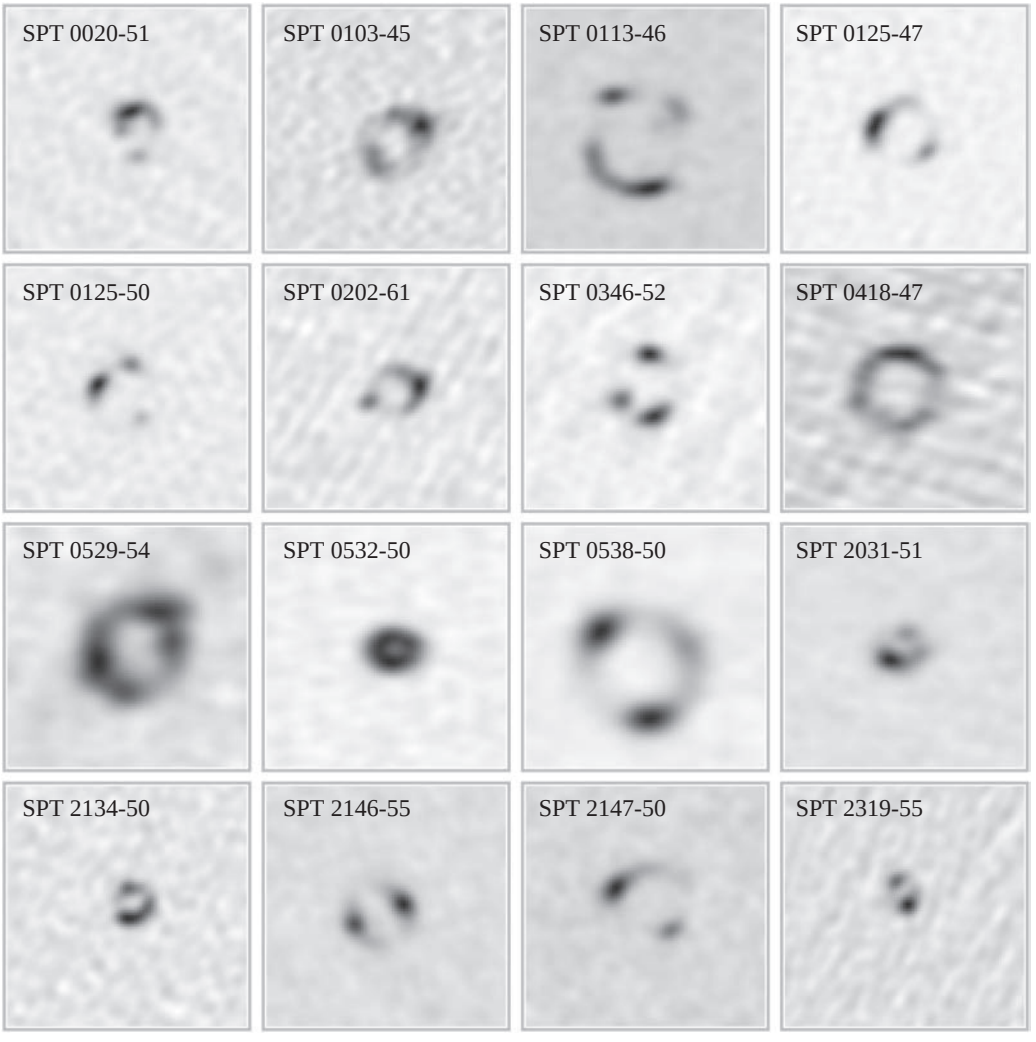

FIGURE 6.4. New lens systems found by the South Pole Telescope and confirmed by ALMA observations. Each panel shows the lensed emission from the background object. (Figure created from ALMA Cycle 0 imaging by J. Vieira, and used with permission. More details can be found in Vieira et al. (2013).)

are nearly all shown to be lens system (Figure 6.4; Vieira et al. 2013). In this case the target refinement of a simple flux cut led to the discovery of several tens of new lens systems. These new lenses were discovered in the first 1300 square degrees of the SPT survey; the full 2500 square degrees should produce a similar number of lenses.

6.4. Substructure in galaxies

6.4.1 *Background*

One of the key methods for investigating galaxy formation, structure and evolution is through computer simulations. These simulations are typically based on the ΛCDM model, whereby cold dark matter (CDM) is the primary matter component in a universe

that is dominated by dark energy. Starting with initial fluctuations in the density field, the simulations predict the formation of structure from early in the history of the Universe until today. These simulations (e.g. Navarro, Frenk & White 1996; Moore et al. 1999; Springel et al. 2005) have done an excellent job in reproducing the large-scale structure of the Universe as revealed by galaxy surveys (e.g. York et al. 2000; Colless et al. 2001). However, at galactic and sub-galactic scales there appear to be serious discrepancies between the observations and the simulations. In addition to the smooth mass distribution of the overall halo, the simulations predict a large amount of substructure in galaxy-scale haloes, where the substructure mass function can be approximated by a power law: $dN/dm \propto m^{-\alpha}$. As an example, Diemand, Kuhlen and Madau (2007) found that $f_{\rm sub} = 5$–10% of the total mass within a virial radius was contained in substructures with masses in the range 4×10^6–$4 \times 10^9\ M_\odot$, and that the slope of the mass function was $\alpha = 1.9 \pm 0.1$. In contrast, the observed mass function (often expressed as a distribution of the maximum circular velocity) of luminous satellites in the Milky Way, where the most complete investigations of substructure have been conducted, has a shallower mass slope ($\alpha \sim 1.0$). This difference in slope leads to the famous 'missing satellite problem', where there appear to be many fewer low-mass Milky Way satellites than predicted (e.g. Moore et al. 1999; Klypin et al. 1999). In addition, there may be some tension on the high-mass end of the satellite distribution, with more large satellites observed in the Milky Way than predicted for the generic galaxy halo (e.g. Strigari et al. 2007).

There have been many solutions proposed for the missing satellite problem. One is that the low-mass substructures are there, but lack a visible stellar component due to a past quenching of star formation (e.g. Mac Low and Ferrara 1999; Dekel and Silk 1986; Bullock, Kravtsov and Weinberg 2000; Benson et al. 2002; Somerville 2002; Mayer et al. 2006). A similar explanation is that these systems are not detected because their stellar population is too spatially diffuse to be detected against the background of Milky Way stars (Bullock et al. 2010). Another, more exciting possibility is that our theory of dark matter is not completely correct, and thus the CDM simulations over-predict the number of substructures. A fourth possibility is that the Milky Way may be an outlier, as could be revealed by substructure searches among larger samples of galaxies.

Heroic efforts have been made to increase the number of detected Milky Way satellites, with most of the recent discoveries being very low surface brightness dwarf satellites (e.g. Zucker et al. 2006a,b; Simon and Geha 2007; Simon et al. 2011; Willman et al. 2011; Kirby et al. 2013; see also the nice summaries in Tollerud et al. 2008 and Madau, Diemand and Kuhlen 2008). These have alleviated somewhat the missing satellite problem. Furthermore, all of the new faint satellites have been found in the SDSS area. Extrapolating from that to the full sky improves the situation further, but still not quite to the level predicted by the simulations. See, for example, Figure 5 in Madau et al. (2008).

Of course, even if the mass distribution of the Milky Way satellites is eventually found to be consistent with the simulations, it is still important to conduct observational tests of the simulations on a larger sample that contains a range of halo masses and galaxy types, as well as spanning a large redshift range to look for evolutionary effects. This becomes more and more difficult as we examine ever more distant galaxies because of the extremely low luminosities of the low-mass satellites. It is here, therefore, that gravitational lensing can provide an excellent complement to the work being done in the local Universe, since lensing has the capability of finding even purely dark satellites, and finding them in cosmologically distant galaxies. As a bonus, the lensing approach can provide a direct measurement of the mass of any detected substructure, allowing a more straightforward comparison to the simulations. The goal in these observations is to make measurements of

the normalization, $f_{\rm sub}$, and slope, α, of the substructure mass function, and to compare these observed values to the predictions of the simulations.

6.4.2 *Overview: lensing techniques for finding substructure*

The presence of lumpy substructure in the halo of a lensing galaxy perturbs the overall lensing potential and, therefore, has the possibility of producing an observable signature of the presence of substructure. These signatures can occur in (1) the fluxes, (2) the positions, or (3) the time delays of the lensed images. I will discuss the basic idea behind each of these directly below, and then go into a bit more detail about each of them in the following sections.

Flux ratio anomalies. The fluxes of lensed images of a distant source depend on the second derivatives of the lensing potential, as described by Suyu (this volume, Chapter 1). To summarize, the magnification of a lensed image is given by the inverse of the Jacobian matrix $\mathcal{A}(\theta)$, where

$$\mathcal{A}(\theta) \equiv \frac{\partial \vec{\beta}}{\partial \vec{\theta}} = \left(\delta_{ij} - \frac{\partial^2 \psi(\theta)}{\partial \theta_k \partial \theta_j} \right)$$

and ψ is the projected and scaled gravitational potential (see the chapter by Suyu). The change in magnification due to the introduction of lumpiness in the mass distribution of the lens can be quite significant, making flux ratio anomalies the easiest to observe of the three effects. In the case of strong lensing by distant galaxies, this effect is most commonly observed as microlensing of quasar images due to the presence of stars in the lensing galaxies. However, it can also be used to search for larger mass substructure with an appropriate choice of observing parameters. This is because the flux perturbation is effective when the angular size of the lensed object is smaller than the Einstein ring radius of the substructure. In order to minimize the effect of microlensing by stars, it is thus necessary to observe the system at a wavelength for which the angular size of the lensed object is larger than the microarcsecond scale of the stars' Einstein rings. For quasars, this is achieved at mid-infrared (mid-IR) and radio wavelengths, but not at optical wavelengths.

Astrometric anomalies. The next easiest perturbation to observe is the shifting of the location of the lensed images. In this case, the effect depends on the first derivatives of the gravitational potential of the lens, since image positions depend on the deflection angle given by $\vec{\alpha}(\vec{\theta}) = \nabla\psi(\vec{\theta})$. In the cases where the background objects are AGN, this effect is expressed by an offset between the observed image position(s) and that/those predicted by a model with a smooth mass distribution. This can be observationally detected if the angular resolution of the observations is on the order of milliarcseconds (mas) or better, as in the case of B0128+357 (Biggs et al. 2004). If the background object is extended and is lensed into a long arc or an Einstein ring, this effect can be seen as small-scale perturbations in the ring emission.

Time delay anomalies. The presence of lumpy mass structure in a galaxy halo can also affect the time delays between lensed images via the 'zeroth derivative' of the gravitational potential, here expressed as the Fermat potential introduced in the chapter by Suyu:

$$\tau(\theta) = \frac{1}{2}(\theta - \beta)^2 - \psi(\theta).$$

Because the time delay depends on the gravitational potential, the full population of substructures can affect each time delay in a given lens system. However, even this cumulative effect is very small, on the order of hours (Keeton and Moustakas 2009) and thus requires a significant improvement in precision in time delay measurements over the ∼1 day uncertainties that are achieved in the best cases to date (e.g. Fassnacht et al. 2002; Tewes et al. 2012).

6.4.3 *Flux ratio anomalies*

As discussed above, the presence of substructure in the lensing galaxy has its strongest observable effect on the fluxes of the lensed images, especially when the lensed object is an AGN. Of course, this effect can be present in any of the lensed images, but the easiest and most robust technique for finding flux perturbations is to look at four-image lens systems that have images that are close together. That is because there are certain generic relationships that govern merging images (i.e. those close together and on either side of the critical line in the lens plane) in the case of a smoothly varying mass distribution. The chapter by Suyu presented these as the fold and cusp relations. Any violation of these relations may indicate the presence of lumpiness (i.e. substructure) in the lensing mass.

The fold relation occurs when the lensed object is close to a fold caustic in the source plane. Two of the lensed images that are produced by this configuration will lie close together on either side of the critical curve. If we could move the lensed source closer and closer to the fold caustic, the sum of the magnifications of the two images would approach zero, i.e. $\mu_A + \mu_B = 0$, for a smooth mass distribution and taking the image parities into account. Because the absolute values of the magnifications will approach equality, $|\mu_A| = |\mu_B|$, the observational effect will be lensed images that approach equal fluxes. Therefore, fluxes that are significantly different may indicate substructure. The left panel of Figure 6.5 shows a violation of the fold relation, although in this case the violation may be due to microlensing by stars in the lensing galaxy.

The cusp relation is produced when the lensed object lies close to a cusp caustic. This will lead to three lensed images close together on the sky, and as we move the source closer to the cusp, the magnifications of the three images approach $\mu_A + \mu_B + \mu_C = 0$, or $|\mu_B| = |\mu_A| + |\mu_C|$, where image B is the middle image Once again, violations of this relation may indicate substructure. The right panel of Figure 6.5 shows a violation of the cusp relation. In this case, since the imaging was done at radio wavelengths and should therefore be insensitive to microlensing, the flux ratio anomaly may very well be due to substructure.

As mentioned above, lumpiness in the mass distribution of the lensing galaxy is routinely observed when observing lensed quasars at optical wavelengths. This lumpiness is, however, due to the presence of the stellar component of the lens. While there are many fruitful investigations that can use this information, including those of the structure of the accretion disc of the lensed object (e.g. Pooley et al. 2007; Poindexter, Morgan and Kochanek 2008; Dai et al. 2010; Mosquera et al. 2013), the microlensing by stars is in essence a contaminating signal if we are looking for CDM substructure. Flux ratio anomalies can also be caused by noise (if the lensed images are faint) or variable extinction across the lensing galaxy caused by dust in the lens. Therefore, to maximize the probability that any flux ratio anomaly is actually due to CDM substructure, we need deep imaging that is as minimally sensitive to dust in the lensing galaxy and to microlensing as possible, while still being sensitive to lensing by CDM substructure. Observations obtained at radio and mid-infrared wavelengths fit these criteria to a large extent. If

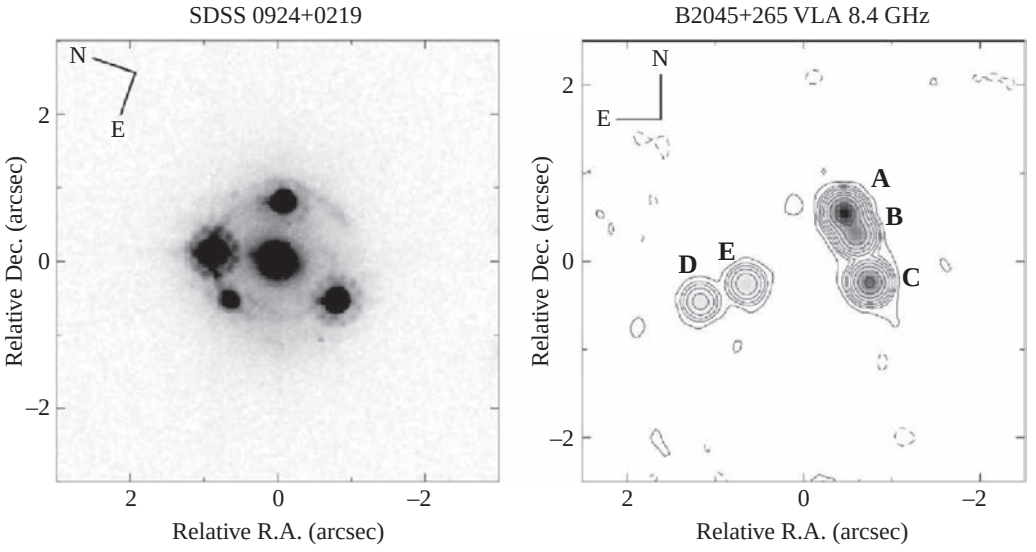

FIGURE 6.5. Examples of violations of generic flux ratio relations. Left: the four-image system SDSS J0924+0219, which shows a fold relation violation. The two leftmost lensed images should have nearly equal fluxes, but one is significantly brighter than the other. Figure shows data obtained with the ACS on *HST*. This violation may be due to microlensing by stars in the lensing galaxy. The figure was made with data that were downloaded from the *HST* archive and processed. The data were originally obtained under programme GO-9744 (PI: Kochanek). Right: the B2045+265 four-image lens system, as imaged by the VLA at 8.4 GHz. Components A–D are the lensed images of the background object, while component E is a radio-loud AGN in the lensing galaxy. This system has perhaps the strongest violation of the cusp relation. Component B should be the brightest of the three close images (A–C), with a flux that is approximately equal to the sum of components A and C. Instead it is the weakest of the three components. (This is Figure 1 of 'B2045+265: A new four-image gravitational lens from CLASS', Fassnacht et al. 1999b, *AJ*, **117**, 658–670. Reproduced by permission of the AAS.)

the lensed objects are AGN, then the angular sizes of their emission regions are on the order of milliarcseconds, comfortably larger than the microarcsecond Einstein ring radii of stars and well matched to the Einstein ring radii of substructures with masses above $\sim 10^{(5-6)} M_{\odot}$.

For around a decade the best sample of lens systems with which to study flux ratio anomalies remained the seven systems from the CLASS programme (Browne et al. 2003; Myers et al. 2003). This sample was originally studied by Dalal and Kochanek (2002). With their statistical analysis, they found $f_{\rm sub} = 0.02$, with a 90% confidence region of $0.006 < f_{\rm sub} < 0.07$.

Clearly there is a need for more systems in order to improve the precision of this technique for studying substructure. However, the CLASS programme, and a similar but smaller survey in the southern hemisphere (Winn et al. 2002), have essentially exhausted the known population of flat-spectrum radio sources as a parent population for a lens survey. This means that until the next deep and wide-area radio survey is conducted, no new large sample of radio-loud quasar lenses is anticipated. However, an alternative approach provides promise: using the increased sensitivity of existing arrays to detect radio emission from 'radio-quiet quasar' lenses (e.g. Jackson 2011). Although much effort is needed to detect these objects, it is not unreasonable with the improved radio arrays. Similarly, mid-IR observations have enormous potential for increasing the sample of useful lens

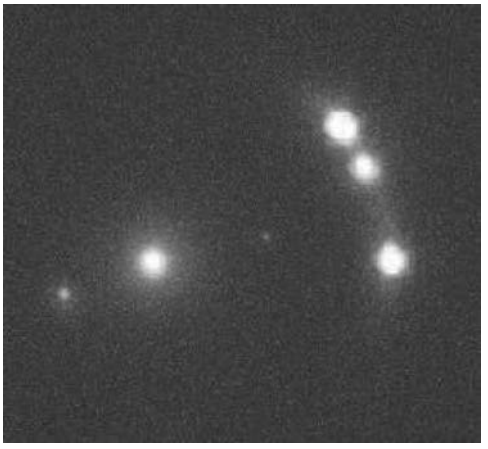

FIGURE 6.6. Adaptive optics imaging of the B2045+265 system, obtained in the K' band with the NIRC2 instrument on the Keck II Telescope. The system shows the four lensed images (labelled A–D in Figure 6.5), the primary lensing galaxy (coincident with component E in Figure 6.5), and a faint galaxy 'G2' between the main lensing galaxy and the three bright lensed images. This galaxy, which is probably a satellite of the primary lens, may be in part responsible for the flux ratio anomaly seen in this system, although to do so requires a very elongated mass distribution for G2. (Figure made from unpublished data that are deeper than those that were originally presented in McKean et al. 2007.)

systems. In the mid-IR, the emission is thought to be coming from dust surrounding the AGN, which should be a common situation. It is very difficult to obtain the necessary sensitivity with ground-based observations (e.g. Chiba et al. 2005), due to the overwhelming thermal emission from the Earth's atmosphere, but space-based observations provide a path forward.

The Dalal and Kochanek (2002) analysis resulted from a statistical treatment of the number and magnitude of flux ratio anomalies in radio-loud quasar lenses. It is possible to take a slightly different approach to systems with known flux ratio anomalies, namely to search for the perturbing object directly with high-resolution imaging. If a substructure is luminous (i.e. a dwarf satellite of the primary lensing galaxy), then measuring its location breaks the modelling degeneracy between a substructure's mass and its distance from the lensed images. The satellite can be incorporated into the lens model and its mass can be determined. This approach has been successfully used with *HST* imaging to explain flux ratio anomalies in MG0414+0534 (Schechter and Moore 1993) and MG2016+112 (Koopmans and Tren 2002). Ground-based adaptive optics (AO) imaging can also be used to locate luminous substructure, as was done by McKean et al. (2007) for the CLASS lens B2045+265, which has the most severe known anomaly (Figures 6.5 and 6.6). However, in that case the mass distribution of the satellite would have to be highly elongated and it remains a distinct possibility that a smaller-mass substructure that is closer to the lensed images is causing the perturbation to the fluxes.

6.4.3.1 Moving into the future

In the very near-term future, with deep radio observations of radio-quiet lens systems and challenging mid-IR observations, it is unlikely that the sample of systems that are well suited for using flux ratio anomalies for investigating substructure will increase by more than a factor of 2 or 3. In order to have a transformative leap in precision, and

to begin to study substructure as a function of galaxy properties or cosmic time, we need new facilities. In the mid-term future, the *James Webb Space Telescope* (*JWST*) should provide the necessary large leap in mid-IR follow-up of new lens samples produced by the current and upcoming sky surveys (e.g. DES, Pan-STARRS, *Euclid* and LSST). The ground-based mid-IR observations of B1422+231, one of the brightest known lensed quasar systems, detected the brightest image (10 mJy) only at a signal-to-noise ratio (SNR) of ∼5 after 3.1 hr with the Subaru Telescope (Chiba et al. 2005). In contrast, the MIRI instrument on *JWST* is projected to achieve SNR = 10 with only 100 s for a much fainter (0.02 mJy) object. This means that doing a snapshot-mode investigation of ∼1000 four-image lens systems is eminently possible.

Farther in the future, the SKA will lead to another huge increase in the number of lens systems suitable for flux-based substructure investigations. As an example, consider the possible SKA programme presented by Koopmans, Browne and Jackson (2004), who discuss the benefits of a 20 000 square degree survey conducted at 1.4 GHz with the SKA. With the proper array configuration and ∼4 min per pointing, this survey could achieve sensitivity of ∼1 μJy over the full survey area in a little under 2 months of full-time observing. The vast majority of sources detected in such a survey would be star-forming galaxies, but even so it would detect $\sim 10^4$ lensed AGN at $z \sim 2$. This would provide an excellent complement to mid-IR imaging obtained with *JWST* and should lead to high-precision determinations of the substructure mass function parameters and, in addition, would provide the opportunity to investigate trends with, for example, galaxy mass, galaxy type and cosmic time.

6.4.4 *Astrometric anomalies and gravitational imaging*

The presence of substructure can perturb the location of the lensed emission. For systems in which the dominant component of the lensed object is an AGN, these perturbations will manifest themselves as a shift in the location of the lensed point sources. In most lens systems these shifts are so small that they can only be detected with mas-scale imaging such as that provided by VLBI radio observations, and may not be detected even in these cases. However, an excellent example of astrometric (and other) anomalies can be seen in the case of the CLASS lens B0128+357, where smooth mass models cannot fit the locations of all four lensed images to within the sub-mas positional errors (Biggs et al. 2004).

In the near-term future, the systems that are most likely to be useful for using astrometric anomalies to search for substructure will be those in which the background object is extended and is lensed into a significant arc or a full ring. In these situations we can search for distortions to the lensed emission due to the gravitational effect of nearby substructure, a technique known as 'gravitational imaging'. This approach starts with a smooth model for the gravitational potential of the lensing object, and then perturbs both the the potential and the surface brightness structure of the background object in order to find the best fit to the observed lensed emission (e.g. Koopmans 2005; Vegetti and Koopmans 2009a). If significant perturbations are required, they may be due to the presence of substructure.

An excellent illustrative example of this technique is shown in Figure 6.7, which shows a high-mass application. A distant galaxy is being lensed by the gravitational potential of a compact galaxy group into a long arc and short counterarc. One of the group members, galaxy G4, lies right on top of the arc, and the perturbation due to G4 causes a gap and splitting to appear in the arc. In this case the cause of this arc morphology is obvious since the luminosity of G4 makes it easily visible in these images. The power of the

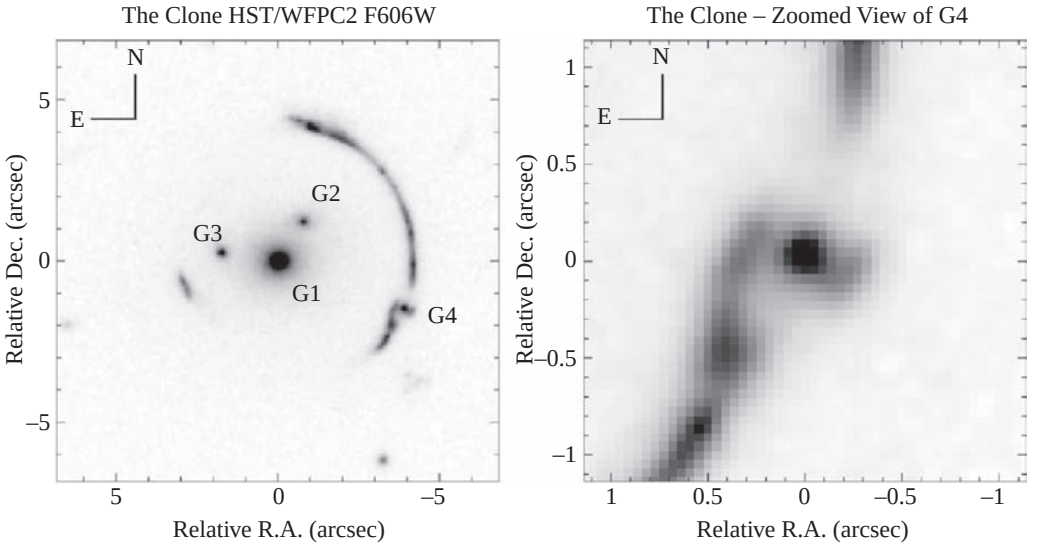

FIGURE 6.7. Space-based imaging, with the WFPC2 camera on *HST*, of the SDSS J120602.09+514229.5 group-scale lens system, otherwise known as the 'Clone', showing a high-mass example of the idea behind the gravitational imaging technique. Galaxies G1–G4 are group members, and the group potential is lensing a blue background galaxy into a long arc on the west side of the group, with a short counterarc on the east side. The presence of G4 causes the arc to have a gap and to be split, as can be seen clearly in the zoomed-in image on the right. These figures were generated from data that were downloaded from the *HST* archive and processed. The data were originally obtained as part of programme GO-11167 (PI:Allam). For a higher-quality image and full description of the analysis, see Vegetti et al. (2010a), who find the mass of G4 to be $(2.75 \pm 0.04) \times 10^{10} M_{\odot}$.

gravitational imaging technique is that even if G4 were too faint, or even purely dark, we could locate it and measure its mass just by its gravitational effect on the arc. Vegetti, Czoske and Koopmans (2010a) have done the analysis on this system and found the mass of G4 to be $(2.75 \pm 0.04) \times 10^{10} M_{\odot}$.

Of course, the Clone is a relatively high-mass lens, with a high-mass perturber. The situation becomes more challenging when the primary lens is a single galaxy and we are searching for substructures with masses $\leq 10^{9} M_{\odot}$. This is because the scale of the morphological perturbations to the lensed emission depends on the mass of the perturber. The lower the mass of the perturber, the higher the required angular resolution for detection of the distortions in the ring/arc morphology. Angular resolutions of tens of milliarcseconds or better are necessary for effective searches for substructure in isolated galaxies, meaning that observations need to be taken with space-based telescopes, adaptive optics systems on ground-based telescopes, or interferometers.

6.4.4.1 Observations confront the simulations

Of course, the goal of detecting substructure by gravitational imaging and other techniques is to use the observations to obtain measurements of the parameters describing the substructure mass function and perhaps to look for signs of evolution in those parameters. An approach to use for this purpose is to start with the simulations and predicted the number of substructures, $N_{\rm det}$, that would be detected in a survey of $N_{\rm lens}$ lens systems. The number of detections depends on the mass function parameter

values, α and $f_{\rm sub}$, as well as the lowest-mass substructure to which the observation is sensitive, $M_{\rm det}$. Expressing this as a conditional probability, the prediction is for:

$$P(N_{\rm det}|\alpha, f_{\rm sub}, M_{\rm det}, N_{\rm lens}).$$

This prediction has to take into account the region of the lensing galaxy being probed by the lensed emission, since tidal effects can lead to disruption of substructure in the innermost regions of galaxy haloes. When the survey has been completed, the actual number of detections can be used in a Bayesian analysis to obtain the posterior probability distribution of α and $f_{\rm sub}$, i.e.

$$P(\alpha, f_{\rm sub}|N_{\rm det}, M_{\rm det}, N_{\rm lens}),$$

which is exactly what we want. Simulations by Vegetti and Koopmans (2009b), showed that the precision of the determinations of α and $f_{\rm sub}$ improves, as expected, as $N_{\rm det}$ increases, as it will as $N_{\rm lens}$ increases and/or $M_{\rm det}$ decreases. Surveys of several tens of lenses are necessary to produce meaningful statistical measurements for reasonable values of $M_{\rm det}$. In turn, the factors that determine $M_{\rm det}$ are:

(i) the signal-to-noise ratio of the lensed emission;
(ii) the angular resolution of the observations, with better resolution leading to lower $M_{\rm det}$ (as discussed above); and
(iii) the morphology of the lensed object, with lumpier morphologies leading to lower $M_{\rm det}$ than smoother surface brightness distributions.

6.4.4.2 Current status of gravitational imaging

Although the observational and modelling requirements for gravitational imaging of subgalactic substructure are stringent, recent work has shown that this method can indeed be successful. With the requirement for high angular resolution, the observational efforts have concentrated on *HST* and adaptive optics imaging. The first of the two main data sets being used in recent work is the SLACS data set, which uses *HST* imaging. As discussed in Section 6.2.3.3, SLACS has found 85 confirmed gravitational lenses via a spectroscopic search through the SDSS data, with follow-up *HST* imaging with either ACS or WFPC2 (Auger et al. 2009). In this sample the lensing galaxies are massive ellipticals, primarily in the redshift range $0.1 < z < 0.3$. The first subgalactic substructure found by the gravitational imaging technique was discovered in SDSSJ0946+1006 (also known as the 'Jackpot' or 'double Einstein ring' lens). The analysis by Vegetti et al. (2010b), found a significant detection of a substructure with a mass of $(3.5 \pm 0.2) \times 10^9 M_\odot$. The lensing galaxy in this system has a redshift of $z_{\rm L} = 0.222$.

The second substructure discovered via gravitational imaging came out of the Strong-lensing High Angular Resolution Programme (SHARP; Lagattuta et al. 2012). This project uses adaptive optics imaging, aided by a laser guide star, with the 10 m Keck Telescopes. Nominally, the angular resolution provided by these observations should be a factor of 4 better than that in observations at similar wavelengths with the 2.5 m *HST*, since for a telescope of diameter D, the angular resolution is $\theta_{\rm lim} \propto \lambda/D$. In practice, resolutions with Keck AO of 60–90 mas are fairly typical. Note that for current AO systems, the performance is best at near-infrared (NIR) wavelengths. Figure 6.8 shows a comparison of the image quality between *HST*/NICMOS (top row) and early SHARP adaptive optics (bottom row) imaging data for five lens systems. The AO data clearly have better angular resolution than the NIR *HST* data. Of course, the contrast should become less severe if optical imaging is available with *HST*. Thus, the AO observations

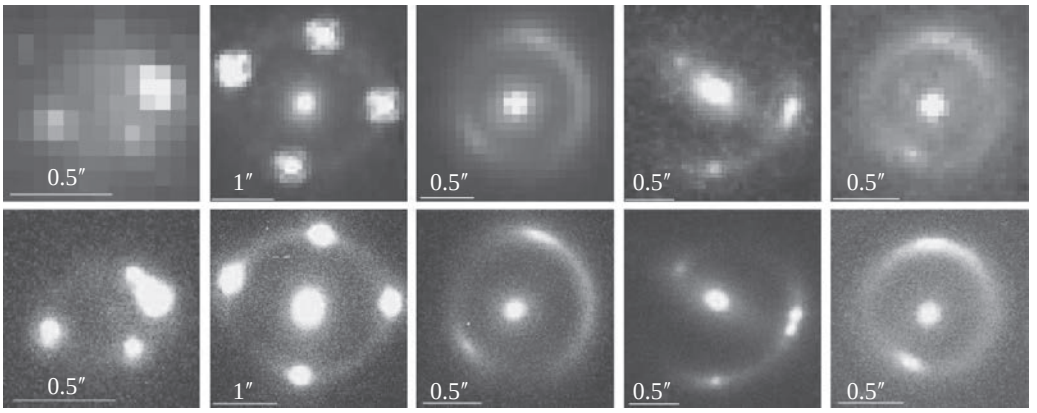

FIGURE 6.8. Early results of imaging from SHARP of five gravitational lens systems. Top row: *HST*/NICMOS F160W imaging. Bottom row: Keck adaptive optics K'-band imaging. In all cases, the adaptive optics imaging is sharper than that obtained with *HST* at these near-infrared wavelengths. Images based on the full-depth data will be presented in Fassnacht et al. (in preparation).

are most critical for lens systems that are very red, either due to dust or from being at high redshift.

This is exactly the situation for the B1938+666 lens system, where the lensing galaxy is at a redshift of $z_{\rm L} = 0.881$ (Tonry and Kochanek 2000) and the background source is at $z_{\rm S} = 2.059$ (Riechers 2011). The lensed emission forms a complete Einstein ring (rightmost column of Figure 6.8). The gravitational imaging analysis of this system revealed the presence of a substructure with mass $(1.9 \pm 0.1) \times 10^8 M_\odot$, similar to that of the Sagittarius dwarf in the Milky Way (Vegetti et al. 2012). This detection was made in three independent data sets, two NIR bands of AO imaging and the NIR *HST*/NICMOS imaging. The power of the technique is shown by the highly significant detection of this substructure (e.g. Figure 6.9) even though it is nearly a factor of 20 less massive and is at a much higher redshift than the detection in the 'Jackpot' system that was discussed above. Owing to the high redshift of the lensed object in the B1938+666 system, the Einstein ring only becomes visible at NIR wavelengths. In this regime, the Keck AO imaging provides better angular resolution than *HST*. Consequently, the significance of the detection in the AO data was higher than that of the *HST* imaging, even in the presence of bright thermal emission from the Earth's atmosphere in the AO data.

In the literature there are now two sub-haloes for galaxy-scale lenses detected via the gravitational imaging technique, SDSSJ0946+1006, where the lens is at $z_{\rm L} = 0.222$, and B1938+666 where the lens is at $z_{\rm L} = 0.881$. Although this is a very small sample, it is still possible to do a rough mass-function analysis with these data. This analysis reveals values of the parameters that are consistent, at least within the 95% confidence regions, with the predictions of the ΛCDM simulations: $\alpha = 1.1^{+0.6}_{-0.4}$ and $f_{\rm sub} = 3.3^{+3.6}_{-1.8}$ (Vegetti et al. 2012). Many current simulations predict substructure fractions of $f_{\rm sub} \leq 1\%$ in the inner 5–10 kpc (projected) of galaxies, so these results are interesting, but certainly do not provide any challenge yet to the predicted values. Also, the lensing galaxies in these systems are more massive than the Milky-Way-sized haloes that are used in many of the simulations (e.g. Diemand et al. 2007), and some work has suggested that $f_{\rm sub}$ should be larger in more massive haloes (e.g. Madau et al. 2008). Clearly the sample size will need to be increased in order to make more meaningful comparisons to the simulations.

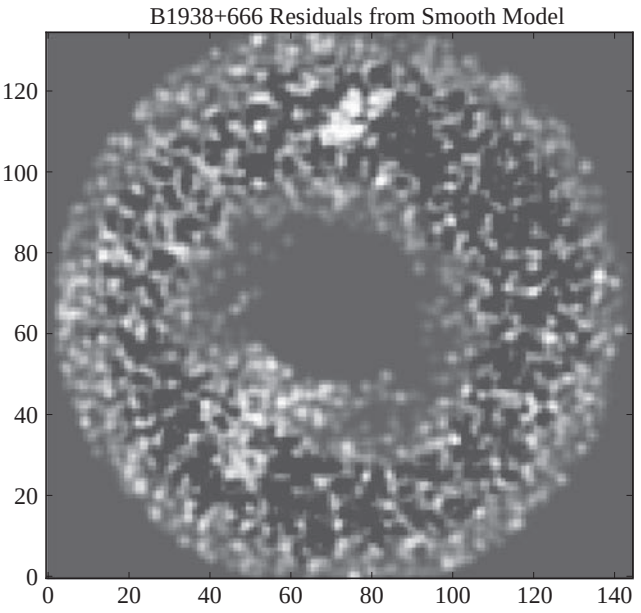

FIGURE 6.9. Difference image between the B1938+666 adaptive optics imaging data (bottom right panel of Figure 6.8) and the best-fitting smooth mass model. This model is presented in Lagattuta et al. (2012) and is used as the initial guess for the modeling in Vegetti et al. (2012). The central galaxy has been subtracted from these data. The smooth mass model clearly does not fully capture the nature of the lensed emission since there are significant residuals, both positive and negative, especially in the northern section of the ring. Instead there is a need for perturbations on small angular scales. Pixels are 0.01 arcseconds in size, so the field of view of this image is 1.45×1.35 arcsecond^2.

6.4.4.3 Moving into the future

In the short-term future of the gravitational imaging technique, the sample of properly analysed systems will grow significantly, with the completion of a 10-system of SLACS lenses (Vegetti et al., in preparation). This will provide an excellent sample at low ($0.1 < z < 0.3$) redshifts. The SLACS systems are also being investigated at UV wavelengths in an ongoing *HST* observational programme (Principal Investigator: Koopmans). Because one of the factors that determines $M_{\rm det}$ is the morphology of the lensed object, this *HST* programme should be able to detect lower-mass substructure in the SLACS lenses by focusing on wavelengths where knots of star formation are more prominent. This is in contrast to the current efforts, which probe the red end of the rest-frame optical emission of the lensed objects, where the morphologies tend to be smoother and thus provide lens sensitivity to low-mass substructure.

To complement the SLACS samples, and to provide the first opportunity to investigate evolution in substructure properties, requires a similar sample at higher redshifts. There are two ongoing programmes that will provide higher redshift probes of galaxy substructure at moderate redshifts. The first is SHARP (Lagattuta et al. 2012; Fassnacht et al., in preparation), which is using adaptive optics and is targeting $0.2 < z_{\rm L} < 1.0$ lens systems. The second is BELLS (Brownstein et al. 2012), which uses the SLACS approach of spectroscopic selection and *HST* follow-up, but targets higher-redshift lenses. Both surveys are producing data that should be well suited for gravitational imaging investigations.

Also in the fairly short-term future, exciting new data sets at wavelengths outside the optical–NIR range should be brought to bear upon this problem. One of these involves

the use of very long baseline interferometry (VLBI) at radio wavelengths. This method is so exciting because the angular resolution provided by VLBI observations is typically on the order of mas, rather than the tens of mas that are seen in AO and current space-based observations. The higher resolutions will provide sensitivity to lower-mass substructures, and the number of detections should increase given the shape of the predicted mass function. Although the number of radio-loud lens systems is currently small, promising data have already been obtained including on MG0414+0534 (MacLeod et al. 2013) and B1938+666 (McKean et al., in preparation). The upcoming radio surveys should vastly increase these numbers, especially once the SKA comes online. A survey such as that proposed by Koopmans et al. (2004) could lead to nearly 10^5 new lenses, where the background object is a star-forming galaxy. When these sources are lensed, they will produce extended arcs and rings similar to what is seen in SLACS.

Gravitational imaging will also benefit greatly from the advent of the Atacama Large Millimetre-Submillimetre Array (ALMA). A significant number of new lens systems are being revealed by large sky surveys at mm and FIR wavelengths (e.g. Vieira et al. 2013). When followed up at higher angular resolution with ALMA, the vast majority of these sources show long arc and ring morphologies (Figure 6.4). Not only are these morphologies very well suited for the gravitational imaging technique, but the ALMA data also contain velocity information that can be exploited to search for substructure. The sub-mm galaxies that are being lensed in these systems have prodigious rates of star formation. The individual velocity slices through the data cube should thus reveal many knots of star formation that would otherwise be blurred together in the continuum maps. These knots of star formation make the morphology of the lensed object less smooth, and thus the ALMA observations should be able to probe farther down the substructure mass function than would otherwise be possible (Hezaveh et al. 2013).

To maximize the expected advances on the observational side, there is now a need for more extensive simulations. The majority of galaxy-scale simulations focus on haloes with masses that are similar to the mass of the Milky Way. This is driven by practical considerations: most of the observational work to date has been done on the satellites of the Milky Way and Andromeda, and simulations of lower-mass haloes allow the exploration of lower-mass substructures, given a fixed number of particles in the simulation. Since the typical lensing galaxy resides in a more massive halo, it would aid the interpretation of the observations to have a more extensive set of modern simulations of massive early-type galaxies. This should be achievable, since the gravitational imaging technique is only probing substructure masses down to $\sim 10^{7-8}\ M_\odot$, a bit larger than the limiting mass in current simulations. A second aspect in which new simulations can contribute is in assessing the likelihood that the sub-haloes detected by gravitational imaging are physically associated with the lensing galaxy rather than lying somewhere else along the line of sight. This is more challenging, since it requires high mass resolution in a cosmological simulation. However, when such a simulation becomes available, we will be able to predict $N_{\rm det}$ properly for a sample of lens systems, i.e. not just based on the properties of the lens galaxy haloes, but incorporating the full line-of-sight effect. The Bayesian analysis will then produce interesting constraints on the nature of galaxy formation in a much more global sense.

6.4.5 *Time-delay anomalies*

The effects of substructure on time delays between lensed AGN images is expected to be on the order of hours (Keeton and Moustakas 2009). These effects are thus virtually impossible to detect with current monitoring programmes, which lack the cadence and flux precisions for the measurements. However, time delay anomalies provide powerful

constraints on substructure, especially when combined with flux ratio and astrometric anomalies, since each of these is sensitive to a different power of the substructure masses (Keeton and Moustakas 2009). Therefore, it is reasonable to consider what could be done to measure time-delay anomalies. This is the basis for a proposal for a space-based dedicated lens monitoring mission: the Observatory for Multi-Epoch Gravitational Lens Astrophysics (OMEGA; Moustakas et al. 2008). This satellite would have very well controlled detectors such that fluxes of the lensed images could be measured to high precision. A small sample of lenses would be intensively monitored, without the night–day or weather-dependent gaps introduced by ground-based monitoring. As a telescope with a sole focus on lens monitoring, the cadence for each system could be much larger than possible from the ground. Simulations of the performance of the proposed system suggest that interesting insights into the nature of dark matter could come out of the mission.

6.5. Cosmology from strong lenses

The most common, but not the only, approach to cosmology with strong galaxy-scale lenses is exploiting the time delays between multiple lensed images of a background AGN. Therefore, this technique will be the main focus of this section. Other techniques include the use of the lensing rate as a function of source redshift (e.g. Turner 1990) and systems in which a single galaxy lenses two separate background objects at different redshifts (Gavazzi et al. 2008; Collett et al. 2012).

6.5.1 *Basics of cosmology from time-delay lenses*

The chapter by Suyu has introduced the concept of time delays between lensed images, and how they can be used to obtain inferences on the values of cosmological parameters. As a brief summary, the additional time taken by the rays forming a lensed image, compared with the travel time along the path the light would have taken in the absence of a lensing object, is

$$\Delta t(\theta;\beta) = (1+z_{\rm L})\frac{D_{\rm L}D_{\rm S}}{cD_{\rm LS}}\left[\frac{1}{2}(\theta-\beta)^2-\psi(\theta)\right].$$

All of the cosmological information is contained in the 'time-delay distance', $D_{\Delta t} \equiv (1+z_{\rm L})(D_{\rm L}D_{\rm S}/D_{\rm LS})$; the distances in the equation are angular diameter distances and thus depend on the system redshifts and H_0 (primarily) as well as $\Omega_{\rm M}$, $\Omega_{\rm DE}$, w, etc., to a lesser extent. To make the cosmological dependence explicit, the angular diameter distance between two redshifts z_i and z_j is given by (e.g. Carroll, Press and Turner 1992):

$$D_{ij} = \frac{c}{H_0(1+z_j)}\left[\frac{{\rm sinn}\left(\sqrt{|\Omega_k|}\int_{z_i}^{z_j}\frac{dz}{E(z)}\right)}{\sqrt{|\Omega_k|}}\right],$$

where

$$E(z) = \sqrt{\Omega_{\rm M}(1+z)^3+\Omega_k(1+z)^2+\Omega_{\rm DE}(1+z)^{3(1+w)}}$$

and ${\rm sinn}(x) = \sin(x)$, x, or $\sinh(x)$ for open, flat and closed cosmologies, respectively. Thus, if a monitoring campaign produces a measurement of time delays for a lens system and if a well-constrained mass model $\tau(\theta;\beta)$ (where the Fermat potential τ is defined above) can be derived from the observed properties of the lensed emission, then the equation can be rearranged to solve for $D_{\Delta t}$ and subsequently for the associated cosmological

parameters:

$$D_{\Delta t} = \frac{c\,\Delta t}{\tau(\theta;\beta)}.$$

This elegant method was first proposed by Refsdal (1964) and attempts to use time-delay lenses to measure cosmological parameters started soon after the discovery of the first lens system in the late 1970s (Walsh et al. 1979). Unfortunately, the history of this method has been beset with some controversy, and it is only recently that many of the systematic effects that plagued earlier efforts have been properly incorporated into the modelling. After briefly describing this history, this section will summarize the current efforts to measure cosmology with time-delay lenses and then present thoughts about future directions.

6.5.2 *A brief history of cosmology from strong lensing*

The discovery of the first strong lens system, Q0957+561 (Walsh et al. 1979), led almost immediately to attempts to use Refsdal's method to measure cosmological parameters. The efforts have focused primarily on H_0 for most of this history, since $D_{\Delta t} \propto 1/H_0$ and is only much more weakly dependent on the other cosmological parameters. However, improvements in measurement precision and modelling techniques have led to the possibility of placing meaningful constraints on curvature and dark energy parameters, and this is the focus of much of the recent work in the field. The impressive advancements in the use of time-delay lenses for cosmology can be seen in the brief history below.

The 1980s and early 1990s: time-delay controversy. Most of the early efforts focused on Q0957+561, both because of its status as the first lens system to be discovered and because the large angular separation between the lensed quasar images ($\sim 6''$) made monitoring with ground-based telescopes easy. Unfortunately, the slow and smoothly varying nature of the light curve and the combination of the >1 year time delay with gaps in the light curve produced when the system was not up at night led to a poorly determined time delay for this system. The community was split between the 'short delay' and 'long delay' camps (see, for example, the discussion in Press, Rybicki and Hewitt 1992; Pelt et al. 1994). The controversy was finally resolved when a sharp change in the light curve made an unambiguous measurement possible (Kundić et al. 1995, 1997).

Mid-1990s to mid-2000s: good time delays, bad models. This period saw the expansion of dedicated lens monitoring programmes to a number of new systems, many of which were better behaved than Q0957+561. This led to several high-precision measurements of lens time delays (e.g. Biggs et al. 1999; Lovell et al. 1998; Fassnacht et al. 1999a, 2002; Burud et al. 2002a,b). However, in spite these robust and uncontroversial time delays, a wide range of values for H_0 were reported, many of which had quoted uncertainties that made the values seem statistically discrepant to a high significance. These discrepancies were due to an oversimplistic approach to the modelling that, to be fair, was driven in most cases by a small number of observational constraints (i.e. just the locations and fluxes of two to four point-like lensed images). The dependence of the time delay on the value of the gravitational potential means that the value of H_0 that is derived from a given lens will depend sensitively on the slope of the potential in the radial range occupied by the lensed images. Most of the modelling in this period assumed a fixed mass density slope that was, in nearly all cases, isothermal ($\rho(r) \propto r^{-2}$). This is a reasonable assumption, as lensing galaxies appear to have density slopes that are *on average* isothermal (e.g. Koopmans et al. 2006). However, there is enough scatter

around that average value so that the assumption of an exactly isothermal profile will introduce a systematic error into the derived values of H_0. Too many of the papers of this period quoted only formal modelling errors without taking the uncertainties due to the mass slope into account, leading to the appearance of sometimes highly discrepant measurements of H_0.

Mid-2000s to today: industrial time delays and good models. Significant advances were made both in measuring time delays and in modelling the lens mass distribution starting in the 2000s. On the time-delay side, monitoring programmes moved from the previous situation of programmes that monitored just one or a few lens systems to ones that exploited the increasing availability of time on 1-m class telescopes to conduct large-scale systematic lens monitoring projects. Some examples of these include the programme carried out with the Small and Moderate Aperture Research Telescope System (SMARTS) telescopes (e.g. Kochanek et al. 2006b), the Liverpool Telescope robotic monitoring project (e.g. Goicoechea et al. 2008) and COSMOGRAIL (the COSmological MOnitoring of GRAvItational Lenses; e.g. Eigenbrod et al. 2005). The COSMOGRAIL project has not only used a network of telescopes to make measurements of at least six lensed AGN, but has also developed analysis techniques to obtain robust measurements of time delays in the presence of microlensing (Tewes, Courbin and Meylan 2013).

The significant increase in the number of high-precision time delays has been matched by improvements in lens modelling code. The improvements in the mass modelling come from incorporating data that have both high angular resolution and high sensitivity. The full information in the surface brightness distribution of the lensed emission for systems with a (nearly) complete Einstein ring, consisting of data contained in thousands of image pixels, is used in an iterative scheme that solves for both the corrections to the lens potential in relation to a smooth mass distribution and the morphology of the lensed object (e.g. Suyu et al. 2009). These models include as a free parameter the mass density slope in the lensing galaxy and are able to put meaningful constraints upon its value. Thus, it is no longer necessary to assume a possibly incorrect mass slope, and what used to be a systematic uncertainty in the modelling is now included properly in the model and is incorporated into the statistical uncertainties. With this approach for a system with a high SNR detection of the ring, the modelling uncertainties can approach just a few per cent.

At this level of precision, other modelling errors come into play. In particular, contributions from the local environment of the lens, i.e. a group or cluster potential, and the full line of sight effect become important. Both local and line-of-sight effects contribute to an external convergence, $\kappa_{\rm ext}$, which needs to be included properly in the lens model. Unless the lens is in a galaxy cluster, which is apparent based on the angular separation of the lensed images, this effect is also at the level of a few per cent to 10%. Thus, it is no longer a sub-dominant contribution to the error budget and must be fully incorporated into the lens model, as discussed below.

6.5.3 *Current status of cosmology from time-delay lenses*

The improvements in the data sets and in the modelling techniques mean that time-delay lenses are finally fulfilling their promise as tools to investigate cosmology. The requirements for a lens to provide a robust and high-precision measurement of cosmological parameters are:

(i) Redshifts of the lensing galaxy and background object, which can often be obtained from spectroscopic observations with 8–10-m class telescopes.

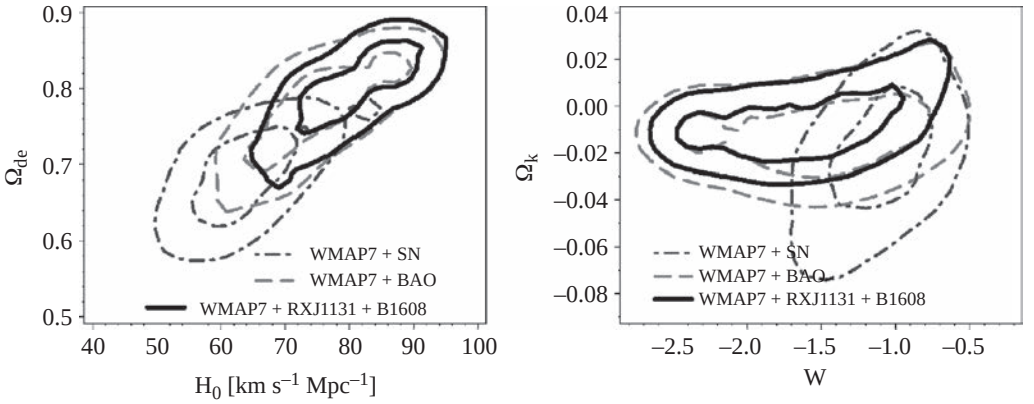

FIGURE 6.10. Constraints on cosmological parameters from three techniques, each of which is combined with data from CMB analyses: lensing (Suyu et al. 2013), supernovae (Hicken et al. 2009), and baryon acoustic oscillations (Percival et al. 2010). The precision from the lensing measurements is comparable in size to the other techniques, providing an independent test for systematic effects in all three approaches. (This is figure 11, 'Two Accurate Time-delay Distances from Strong Lensing: Implications for Cosmology', Suyu et al. 2013, *ApJ*, **766**, article 70, 19 pp. Reproduced by permission of the AAS.)

(ii) High-precision time delays. Currently these have come from radio monitoring (e.g. Fassnacht et al. 2002) or systematic optical monitoring (e.g. Kochanek et al. 2006b; Tewes et al. 2012).

(iii) Improved lens modelling that incorporates the full surface brightness distribution of the lensed emission, as discussed above.

(iv) The stellar velocity dispersion of the lensing galaxy, which is used to assess the mass-sheet degeneracy arising from the local environment of the lensing galaxy (e.g. Suyu et al. 2010).

(v) An estimate of the line-of-sight contribution, which is used to construct a prior for $\kappa_{\rm ext}$ that enters into the Bayesian analysis. One way to do this is to take the $\kappa_{\rm ext}$ distribution obtained by ray-tracing random lines of sight though a large cosmological simulation (e.g., Hilbert et al. 2009), which gives a global distribution. This can be improved upon by incorporating observed information, such as galaxy number counts (Fassnacht, Koopmans and Wong 2011), about the line of sight to a given lens system. These additional data can then be used to select lines of sight through the simulation with similar properties, and an individualized $\kappa_{\rm ext}$ prior distribution can be calculated for that particular lens (e.g. Suyu et al. 2010, 2013).

Currently there are only two lens systems that satisfy all of these conditions: B1608+656 and RX J1131−1231. The analysis of these two systems (Suyu et al. 2010, 2013) has, when combined, yielded constraints that are complementary to and comparable in precision to other major efforts to investigate cosmological parameters (Figure 6.10). Lensing is independent of the other methods and, therefore, can be used to test for systematic errors in the parameter determinations. Additionally, because each lens system provides an independent measurement of these parameters, and because the lens and source redshifts differ from system to system, the precision of the lens-based measurements improves roughly as $\sqrt{N}$ as the sample size increases. There is therefore a strong motivation to increase the number of systems for which the five requirements above are satisfied.

6.5.4 *Moving into the future*

Efforts are well under way to increase, in the very near future, the number of well-characterized time-delay systems from two to five. This increase in sample size will not only improve the precision of the cosmological parameter measurements but also, because each lens system provides an independent probe of cosmology, with a sample of five it will be possible to test for previously unknown systematic effects in the time-delay approach. The additional three systems all have high-precision time-delay measurements and the system redshifts are known. An approved *HST* programme (Principal Investigator: Suyu) is acquiring the high-resolution imaging that is necessary for the mass modelling of the primary lensing galaxies in the three systems, and spectroscopy and multi-band imaging have been acquired to assess the contributions of the local environments and line-of-sight structure to the lens model. Advances have also been made in the interpretation of observational data with regards to the $\kappa_{\rm ext}$ estimation (Greene et al. 2013; Collett et al. 2013). As an example, Greene et al. (2013) show that using stellar mass and photometric redshift estimates derived from multi-band imaging and incorporating the projected distance of each galaxy in the field from the lens system can lead to a reduction in the width of the $\kappa_{\rm ext}$ distribution over the number-count approach used for B1608+656 and RX J1131−1231. These new techniques will be incorporated into the five-lens analysis.

One of the main motivations driving observational cosmology today is the quest to understand dark energy. Already time-delay lenses are contributing to this research, although the uncertainties on the dark energy parameters are still large (Figure 6.10). Further in the future lens-based measurements will really start to contribute to dark energy investigations. The large upcoming surveys should produce hundreds, if not thousands, of quasar lenses. Projections show that if these systems can produce similar results to those derived from B1608+656 and RX J1131−1231, precisions of $\sim$1% or better can be achieved on the dark energy equation of state parameter, w (Coe and Moustakas 2009). Similarly, incorporating lens-based measurements into determinations of w and its rate of change (w_a) provides a significant improvement over just using the next-generation supernovae data. Linder (2011) found that the combination of lensing, supernovae and CMB data can measure dark energy parameters five times better than supernovae plus CMB alone in the presence of curvature. The improvements in the dark energy figure of merit come from the slight tilt between the lens-based and supernova-based confidence regions in the (w, w_a) plane.

The challenge for the lensing community will be turning the hundreds of newly discovered quasar lenses into measurements of cosmological parameters. The first consideration is the time-delay measurements. Important considerations in measuring delays for a large number of systems include the cadence (how often the system is observed), season length and number of seasons for the monitoring. This last point is very important in the presence of microlensing (e.g. Tewes et al. 2012). On the practical side, one approach to measuring a large number of time delays is to use the survey observations themselves. This method can work for the LSST, where the survey observations are designed with a time-domain component from the start. Thus, each field will be revisited hundreds of times over the 10-year project lifetime. Different fields will have different cadences, and the effect of cadence needs to be explored. An interesting test will be if it is possible to measure a high-precision time delay using multi-filter data, since the cadence will be much higher when all filters are included in the data set. This will require a careful modelling of wavelength-dependent variability in AGN. Another consideration for the LSST is that the observing season for a typical field may be fairly short, on the order of a couple of months. Although this seems at first sight to be problematic, initial simulations

indicate that the 10-year monitoring of each field may allow high-precision delays to be measured even with short seasons.

The other approach to measuring hundreds of time delays or more is to utilize a dedicated 1–2-m class telescope or network of telescopes. The success of, e.g., the COSMOGRAIL programme has shown that these telescopes can produce excellent results (e.g., Tewes et al. 2012). However, in order to overcome microlensing effects it is necessary to have a ∼5-year commitment to a monitoring programme, which can be difficult to achieve in the normal process of proposals to a time allocation committee. Thus, securing access on 5-year time scales to small telescopes will be a key component in moving to the future of lens-based cosmology.

The second consideration in using the new large lens samples for cosmology is how to obtain the data that will be used for modelling. Possible avenues to the high-resolution and high-sensitivity imaging of the Einstein ring emission are the JWST and adaptive optics with existing and upcoming telescopes. For the stellar velocity dispersions of the lensing galaxy, spectroscopy with 8–30-m class telescopes will have to be employed. With a well-designed slit mask these spectroscopic observations can also be used to obtain redshifts of nearby galaxies, in order to assess the contribution of the local environment to the lensing potential. The line-of-sight component will probably be estimated from the survey data themselves, since the large optical/NIR surveys will provide colour information about galaxies in the fields of view containing the lens system. With colours, both the photometric redshifts and the stellar masses of these nearby galaxies can be estimated, and subsequently incorporated into a prior distribution for $\kappa_{\rm ext}$. Overall, both the time delay and modelling sides will require substantial effort, but not significantly more than the other techniques that will be used investigate dark energy.

6.6. Concluding remarks

Although this chapter has been somewhat focused, the other chapters have provided a taste of the rich variety of science that can be explored with gravitational lensing. In the vast majority of cases, the science will benefit greatly from the expected orders of magnitude increase in the number of known lenses. The combination of large sky surveys and enhanced follow-up capabilities means that the future of lensing is bright.

Acknowledgements

I am extremely grateful to the organizers of this Winter School, Evencio Mediavilla, Pepe Muñoz and Francisco Garzón, for inviting me to the School and providing a very pleasant experience. I am also grateful to the Instituto de Astrofísica de Canarias and its Director, Professor Francisco Sánchez, for the hospitality shown by the Institute during my visit to the Canary Islands. Special thanks need to go to Lourdes González Pérez for her work in taking care of the organizational details of the School. I am deeply indebted to my long-time collaborators Leon Koopmans, Phil Marshall, Sherry Suyu and Tommaso Treu for many useful and interesting discussions, and in particular about the future of strong lensing.

REFERENCES

Abell, P. A. et al. 2009, arXiv:0912.0201

Auger, M. W. et al. 2009, *ApJ*, **705**, 1099

Bahcall, J. N. et al. 1992, *ApJ*, **387**, 56

Bayliss, M. B. et al. 2011, *ApJL*, **727**, L26
Benson, A. J., Lacey, C. G., Baugh, C. M., Cole, S. & Frenk, C. S. 2002, *MNRAS*, **333**, 156
Biggs, A. D. et al. 1999, *MNRAS*, **304**, 349
Biggs, A. D. et al. 2004, *MNRAS*, **350**, 949
Bolton, A. S., Burles, S., Schlegel, D. J., Eisenstein, D. J. & Brinkmann, J. 2004, *AJ*, **127**, 1860
Bolton, A. S., Burles, S., Koopmans, L. V. E., Treu, T. & Moustakas, L. A. 2006, *ApJ*, **638**, 703
Browne, I. W. A., Wilkinson, P. N., Patnaik, A. R. & Wrobel, J. M. 1998, *MNRAS*, **293**, 257
Browne, I. W. A. et al. 2003, *MNRAS*, **341**, 13
Brownstein, J. R. et al. 2012, *ApJ*, **744**, 41
Bullock, J. S., Kravtsov, A. V. & Weinberg, D. H. 2000, *ApJ*, **539**, 517
Bullock, J. S., Stewart, K. R., Kaplinghat, M., Tollerud, E. J. & Wolf, J. 2010, *ApJ*, **717**, 1043
Burud, I. et al. 2002a, *A&A*, **383**, 71
Burud, I. et al. 2002b, *A&A*, **391**, 481
Cabanac, R. A. et al. 2007, *A&A*, **461**, 813
Carlstrom, J. E. et al. 2011, *PASP*, **123**, 568
Carroll, S. M., Press, W. H. & Turner, E. L. 1992, *ARA&A*, **30**, 499
Chiba, M., Minezaki, T., Kashikawa, N., Kataza, H. & Inoue, K. T. 2005, *ApJ*, **627**, 53
Coe, D. & Moustakas, L. A. 2009, *ApJ*, **706**, 45
Colless, M. et al. 2001, *MNRAS*, **328**, 1039
Collett, T. E., Auger, M. W., Belokurov, V., Marshall, P. J. & Hall, A. C. 2012, *MNRAS*, **424**, 2864
Collett, T. E. et al. 2013, *MNRAS*, **432**, 679
Dai, X. et al. 2010, *ApJ*, **709**, 278
Dalal, N. & Kochanek, C. S. 2002, *ApJ*, **572**, 25
Dekel, A. & Silk, J. 1986, *ApJ*, **303**, 39
Diemand, J., Kuhlen, M. & Madau, P. 2007, *ApJ*, **667**, 859
Eigenbrod, A. et al. 2005, *A&A*, **436**, 25
Eisenstein, D. J. et al. 2011, *AJ*, **142**, 72
Fassnacht, C. D. et al. 1999a, *ApJ*, **527**, 498
Fassnacht, C. D. et al. 1999b,*AJ*, **117**, 658
Fassnacht, C. D., Xanthopoulos, E., Koopmans, L. V. E. & Rusin, D. 2002, *ApJ*, **581**, 823
Fassnacht, C. D. et al. 2004, *ApJL*, **600**, L155
Fassnacht, C. D., Koopmans, L. V. E. & Wong, K. C. 2011, *MNRAS*, **410**, 2167
Faure, C. et al. 2008, *ApJS*, **176**, 19
Gavazzi, R., Treu, T., Koopmans, L. V. E., Bolton, A. S., Moustakas, L. A., Burles, S. & Marshall, P. J. 2008, *ApJ*, **677**, 1046
Gavazzi, R., Treu, T., Marshall, P. J., Brault, F. & Ruff, A. 2012, *ApJ*, **761**, 170
Goicoechea, L. J. et al. 2008, *New Astron.*, **13**, 182
Greene, Z. S. et al. 2013, *ApJ*, **768**, 39
Hennawi, J. F. et al. 2008, *AJ*, **135**, 664
Hewitt, J. N. et al. 1989, *Gravitational Lenses*, **330**, 147
Hezaveh, Y. et al. 2013, *ApJ*, **767**, 9
Hicken, M. et al. 2009, *ApJ*, **700**, 1097
Hilbert, S., Hartlap, J., White, S. D. M. & Schneider, P. 2009, *A&A*, **499**, 31
Inada, N. et al. 2008, *AJ*, **135**, 496
Inada, N. et al. 2010, *AJ*, **140**, 403

Inada, N. et al. 2012, *AJ*, **143**, 119
Jackson, N. 2008, *MNRAS*, **389**, 1311
Jackson, N. 2011, *ApJL*, **739**, L28
Keeton, C. R. & Moustakas, L. A. 2009, *ApJ*, **699**, 1720
Kirby, E. N. et al. 2013, *ApJ*, **770**, 16
Klypin, A., Kravtsov, A. V., Valenzuela, O. & Prada, F. 1999, *ApJ*, **522**, 82
Kochanek, C. S., Mochejska, B., Morgan, N. D. & Stanek, K. Z. 2006a, *ApJL*, **637**, L73
Kochanek, C. S. et al. 2006b, *ApJ*, **640**, 47
Koopmans, L. V. E. 2005, *MNRAS*, **363**, 1136
Koopmans, L. V. E., Browne, I. W. A. & Jackson, N. J. 2004, *New Astron. Rev.*, **48**, 1085
Koopmans, L. V. E. & Treu, T. 2002, *ApJL*, **568**, L5
Koopmans, L. V. E., Treu, T., Bolton, A. S., Burles, S. & Moustakas, L. A. 2006, *ApJ*, **649**, 599
Kundić, T. et al. 1995, *ApJL*, **455**, L5
Kundić, T. et al. 1997, *ApJ*, **482**, 75
Lacki, B. C., Kochanek, C. S., Stanek, K. Z., Inada, N. & Oguri, M. 2009, *ApJ*, **698**, 428
Lagattuta, D. J. et al. 2012, *MNRAS*, **424**, 2800
Laureijs, R. et al. 2011, arXiv:1110.3193
Linder, E. V. 2011, *Phys. Rev. D*, **84**, 123529
Lintott, C. J. et al. 2008, *MNRAS*, **389**, 1179
Lovell, J. E. J. et al. 1998, *ApJL*, **508**, L51
MacLeod, C. L., Kochanek, C. S. & Agol, E. 2009, *ApJ*, **699**, 1578
MacLeod, C. L, Jones, R., Agol, E. & Kochanek, C. S. 2013, *ApJ*, **773**, 35
Mac Low, M.-M. & Ferrara, A. 1999, *ApJ*, **513**, 142
Madau, P., Diemand, J. & Kuhlen, M. 2008, *ApJ*, **679**, 1260
Maoz, D. et al. 1993, *ApJ*, **409**, 28
Marshall, P. J. et al. 2009, *ApJ*, **694**, 924
Mayer, L., Mastropietro, C., Wadsley, J., Stadel, J. & Moore, B. 2006, *MNRAS*, **369**, 1021
McKean, J. P. et al. 2007, *MNRAS*, **378**, 109
Moore, B. et al. 1999, *ApJL*, **524**, L19
Mosquera, A. M. et al. 2013, *ApJ*, **769**, 53
Moustakas, L. A. et al. 2008, *SPIE*, **7010**, 41
Myers, S. T. et al. 2003, *MNRAS*, **341**, 1
Navarro, J. F., Frenk, C. S. & White, S. D. M. 1996, *ApJ*, **462**, 563
Oguri, M. et al. 2006, *AJ*, **132**, 999
Oguri, M. et al. 2008, *AJ*, **135**, 512
Patnaik, A. R., Browne, I. W. A., Wilkinson, P. N. & Wrobel, J. M. 1992, *MNRAS*, **254**, 655
Pelt, J., Hoff, W., Kayser, R., Refsdal, S. & Schramm T. 1994, *A&A*, **286**, 775
Percival, W. J. et al. 2010, *MNRAS*, **401**, 2148
Pindor, B. 2005, *ApJ*, **626**, 649
Poindexter, S., Morgan, N. & Kochanek, C. S. 2008, *ApJ*, **673**, 34
Pooley, D., Blackburne, J. A., Rappaport, S. & Schechter, P. L. 2007, *ApJ*, **661**, 19
Press, W. H., Rybicki, G. B. & Hewitt, J. N. 1992, *ApJ*, **385**, 404
Refsdal, S. 1964, *MNRAS*, **128**, 307
Riechers, D. A. 2011, *ApJ*, **730**, 108
Ruff, A. J. et al. 2011, *ApJ*, **727**, 96
Schechter, P. L. & Moore, C. B. 1993, *AJ*, **105**, 1

Schneider, D. P. et al. 2010, *AJ*, **139**, 2360
Simon, J. D. & Geha, M. 2007, *ApJ*, **670**, 313
Simon, J. D. et al. 2011, *ApJ*, **733**, 46
Scoville, N. et al. 2007, *ApJS*, **172**, 1
Somerville, R. S. 2002, *ApJL*, **572**, L23
Springel, V. et al. 2005, *Nature*, **435**, 629
Strigari, L. E. et al. 2007, *ApJ*, **669**, 676
Suyu, S. H. et al. 2009, *ApJ*, **691**, 277
Suyu, S. H. et al. 2010, *ApJ*, **711**, 201
Suyu, S. H. et al. 2013, *ApJ*, **766**, 70
Tewes, M., Courbin, F. & Meylan, G. 2012, arXiv:1208.5598
Tewes, M., Courbin, F. & Meylan, G. 2013, *A&A*, **553**, A120
Tollerud, E. J., Bullock, J. S., Strigari, L. E. & Willman, B. 2008, *ApJ*, **688**, 277
Tonry, J. L. & Kochanek, C. S. 2000, *AJ*, **119**, 1078
Turner, E. L. 1990, *ApJL*, **365**, L43
Vegetti, S. & Koopmans, L. V. E. 2009a, *MNRAS*, **392**, 945
Vegetti, S. & Koopmans, L. V. E. 2009b, *MNRAS*, **400**, 1583
Vegetti, S., Czoske, O. & Koopmans, L. V. E. 2010a, *MNRAS*, **407**, 225
Vegetti, S., Koopmans, L. V. E., Bolton, A., Treu, T. & Gavazzi, R. 2010b, *MNRAS*, **408**, 1969
Vegetti, S. et al. 2012, *Nature*, **481**, 341
Vieira, J. D. et al. 2013, *Nature*, **495**, 344
Walsh, D., Carswell, R. F. & Weymann, R. J. 1979, *Nature*, **279**, 381
Wilkinson, P. N., Browne, I. W. A., Patnaik, A. R., Wrobel, J. M. & Sorathia, B. 1998, *MNRAS*, **300**, 790
Willman, B. et al. 2011, *AJ*, **142**, 128
Winn, J. N. et al. 2002, *AJ*, **123**, 10
Wisotzki, L., Schechter, P. L., Bradt, H. V., Heinmüller, J. & Reimers, D. 2002, *A&A*, **395**, 17
York, D. G. et al. 2000, *AJ*, **120**, 1579
Zucker, D. B. et al. 2006a, *ApJ*, **643**, L103
Zucker, D. B. et al. 2006b, *ApJ*, **650**, L41